Synthesis and characterization of a new trifunctional magnetic–photoluminescent–oxygen-sensing nanomaterial

2008 Nanotechnology 19 495709

(http://iopscience.iop.org/0957-4484/19/49/495709)

Nanotechnology **19** (2008) 495709 (8pp) doi:10.1088/0957-4484/19/49/495709

Synthesis and characterization of a new trifunctional magnetic–photoluminescent–oxygen-sensing nanomaterial

Lina Liu[1,2], Bin Li[1,4], Jun Ying[3], Xiudong Wu[3], Haifeng Zhao[1], Xinguang Ren[1], Dongxia Zhu[3] and Zhongmin Su[3,4]

[1] Key Laboratory of Excited State Processes, Changchun Institute of Optics, Fine Mechanics and Physics, Chinese Academy of Sciences, 16 Eastern South-Lake Road, Changchun 130033, People's Republic of China
[2] Graduate School of the Chinese Academy of Sciences, Chinese Academy of Sciences, Beijing 100039, People's Republic of China
[3] Polyoxometalate Science Key Laboratory of Ministry of Education, Faculty of Chemistry, Northeast Normal University, Changchun 130024, People's Republic of China

E-mail: lib020@ciomp.ac.cn and zmsu@nenu.edu.cn

Received 13 September 2008, in final form 8 October 2008
Published 19 November 2008
Online at stacks.iop.org/Nano/19/495709

Abstract

Magnetic Fe_2O_3 nanoparticles coated with SiO_2 chemically doped with a Ru(II) complex were prepared using a simple solution based method. Field-emission scanning electron microscopy (FE-SEM) and transmission electron microscopy (TEM) showed that the Fe_2O_3 nanoparticles with a mean diameter of ∼115 nm were successfully coated with Ru(II) complex–chemically doped SiO_2 shell with a thickness of ∼30 nm. The obtained nanocomposite material showed a strong magnetic response to a varying magnetic field, exhibited the bright red triplet metal-to-ligand charge transfer (^{3}MLCT) emission, and its photoluminescent intensity was sensitive to oxygen concentration. Compared with the Ru(II) complex in silica gels, the Ru(II) complex in the magnetic–optical–oxygen-sensing nanocomposite demonstrated improved thermodynamic stability of emissions. These nanocomposites are also nontoxic and easily conjugated with biomolecules. Their magnetic, photoluminescent and oxygen-sensing properties make them promising candidates for cell separation, biomarkers and optical oxygen sensors, which can measure the O_2 concentration in biological bodies.

S Supplementary data are available from stacks.iop.org/Nano/19/495709

1. Introduction

In recent years, considerable effort has been devoted to the design and controlled fabrication of functional nanostructured and nanocomposite materials [1–6]. Magnetic iron oxide nanoparticles are widely used in biomedical applications, such as drug targeting [7], cell sorting and isolation [8], enzyme immobilization [9], and magnetic resonance imaging [10], since they are much less toxic than their metallic counterparts and have high saturation magnetization and superparamagnetic behavior [11]. In order to prevent aggregation and append novel function, it is therefore important that the bare magnetic nanoparticles are coated with a suitable material. Amorphous silica is nontoxic, highly compatible with biological systems, and is usually used as a food additive and component of vitamin supplements [12]. The surface of silica is easily conjugated with amines, thiols and carboxyl groups, which in turn would facilitate the linking of biomolecules such as biotin and avidin. Silica-coated magnetic nanoparticles have been studied by many groups [13–15]. Optical materials are also of great importance in the fields of biology, medical sciences and biotechnology [16–18]. The combination of magnetic and fluorescent materials into a single micro- or nanocomposite system might greatly enhance their application in the biomedical and biopharmaceutical fields. Among the optical materials being investigated for such composites, organic

[4] Author to whom any correspondence should be addressed.

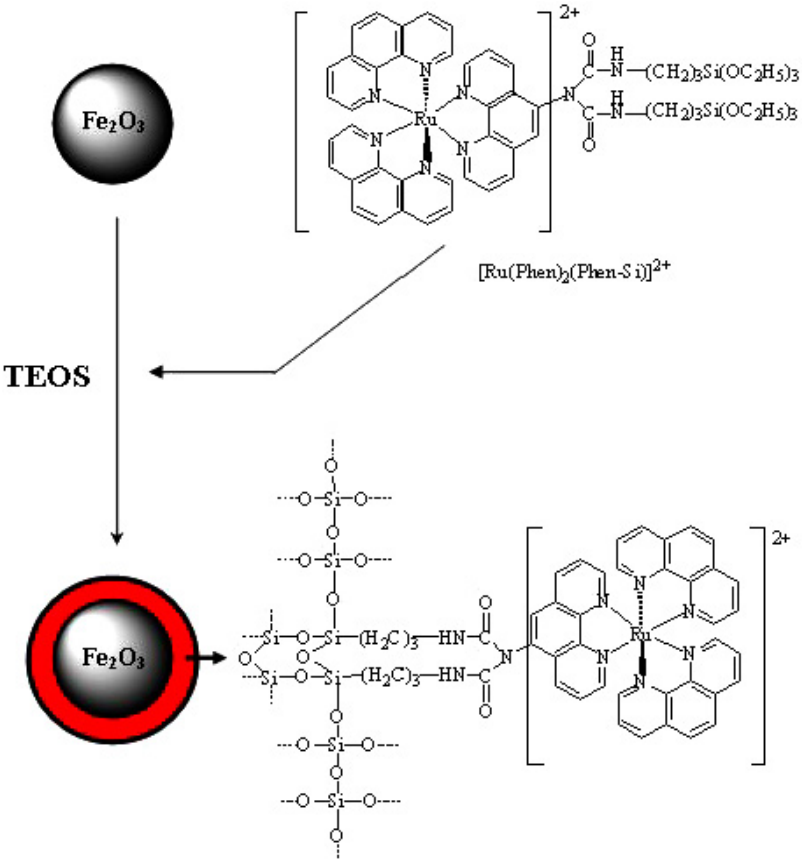

Figure 1. Schematic diagram of the synthetic procedure.
(This figure is in colour only in the electronic version)

small molecular dyes [19] and quantum dots (QDs) [20] are the most widely used fluorescent labels. But both of these have inherent limitations. For example, organic small molecular dyes typically undergo rapid photobleaching [21], whereas QDs are less chemically stable and are potentially toxic [22]. Therefore, it is necessary to find substitutes for current luminescently labeled materials. A few groups have used luminescent rare earth complexes as optical materials in this kind of nanocomposite material [23, 24], but it is hard to avoid phase separation of rare earth complexes in silica because the rare earth complexes used are usually insoluble in a water/ethanol system. The photoluminescent signals of the Ru(II) complex have strong fluorescence intensity and excellent photostability [21, 25]. The Ru(II) complex is soluble in water and ethanol, and can therefore be easily doped in a silica matrix. Furthermore, Ru(II) polypyridyl compounds have been frequently utilized as oxygen-sensitive dyes owing to their highly emissive metal-to-ligand charge transfer (MLCT) state, long fluorescence lifetime, large Stokes shift, high photochemical stability, high sensitivity to oxygen and strong visible absorption in the blue-green region. Virtually all complexes used as sensing probes should be supported on an inorganic or organic polymer matrix due to their intensive self-quenching. Furthermore, the covalently grafting strategy between the SiO_2 matrix and the Ru(II) complex usually shows better optical oxygen properties than those obtained by the physically entrapped method [26, 27]. Importantly, their excitation wavelength is in the visible region, which effectively avoids ultraviolet injury to human tissues. In this paper, we prepared magnetic nanoparticles coated with silica chemically doped with Ru(II) complex. Magnetic, optical and oxygen-sensing functions are combined into a single nanoparticle. The thermodynamic stability of emissions is improved in the magnetic–photoluminescent–oxygen-sensing materials. They are expected to find applications in biomedical and biopharmaceutical fields.

2. Experimental details

2.1. Materials and syntheses

3-(Triethoxysilyl)propyl isocyanate (TEPIC) and the 5% Pd/C catalyst were purchased from Aldrich (Milwaukee, WI, USA) and used as-received. Anhydrous $RuCl_3$ (99.99%) was obtained from Acros Organics (Geel, Belgium). The complex $Ru(Phen)_2Cl_2{\cdot}2H_2O$ was synthesized and purified as described in the literature [28]. $NH_3{\cdot}H_2O$, TEOS, $FeCl_3{\cdot}6H_2O$, 2-propanol, hexane, chloroform and ethanol were obtained from Beijing Chemical Company. The water used in our present work was deionized.

The synthesis of the nanocomposite materials is shown in figure 1. $[Ru(Phen)_2Phen–Si]Cl_2$ complex (Phen: 1,10-phenanthroline) and Fe_2O_3 were first prepared. Then tetra-ethoxysilane (TEOS) together with $[Ru(Phen)_2Phen–Si]Cl_2$

hydrolyzed on the surface of Fe_2O_3 to form a silica shell with a covalently linked ruthenium(II) complex.

2.1.1. Preparation of Phen–Si. The Phen–Si was prepared using 5-amino-1,10-phenanthroline (Phen-NH_2) and TEPIC as the starting materials [29]. The synthesis of Phen-NH_2 was performed by nitration of 1,10-phenanthroline in a mixture of concentrated sulfuric acid and fuming nitric acid, followed by reduction of the nitro derivative with hydrazine over a 5% Pd/C catalyst. Analysis for Phen–Si: NMR ($CDCl_3$): δ 0.52 (m, 4H), 1.13 (t, 18 H), 1.60 (m, 4H), 3.22 (m, 4H), 3.69 (q, 12 H), 7.25 (br s, 2H), 7.61 (m, 2H), 7.81 (s, 1H), 8.18 (m, 2H), 9.15 ppm (m, 2 H). IR (KBr, cm^{-1}): C=O (1710 cm^{-1}), –CONH– (1653, 1541 cm^{-1}), C–Si (1193 cm^{-1}).

2.1.2. Preparation of [Ru(Phen)$_2$ Phen–Si]Cl$_2$. The complex [Ru(Phen)$_2$Phen–Si]Cl_2 was synthesized by modifying a reported procedure [30]. A mixture of Ru(Phen)$_2Cl_2$ and Phen–Si in anhydrous ethanol was refluxed for 8 h in a nitrogen atmosphere to give a transparent deep red solution, indicating that the complexation reaction between Phen–Si and Ru(Phen)$_2Cl_2$ had finished. The molar ratio of Phen–Si to Ru(Phen)$_2Cl_2$ was 1.01:1. Finally the ethanol was rotary evaporated off and the residue was recrystallized by vapor diffusion of diethyl ether into its ethanol solution and dried in a vacuum. [Ru(Phen)$_2$Phen–Si]Cl_2 complex was labeled as sample Ru.

2.1.3. Synthesis of Fe_2O_3 nanoparticles. Fe_2O_3 nanoparticles, labeled as sample Fe were prepared according to literature methods [31]. 2.0×10^{-2} M $FeCl_3$ aqueous solution was aged at 100 °C for 2 days. Then the solution was cooled to room temperature naturally. The product was collected and washed with deionized water and absolute alcohol several times and dried in a vacuum at 80 °C for 4 h.

2.1.4. Synthesis of luminescent magnetic nanocomposite materials. In a typical synthesis, to a solution of 0.45 M ammonia and 3.05 M water in 2-propanol, 72.7 mM Fe_2O_3 nanoparticles was added. Then the solution was put at an ultrasonic bath for 2 h at room temperature. 2×10^{-3} M TEOS and sample Ru (100 mg g^{-1} SiO_2) were added to the solution. The solution was put at an ultrasonic bath for 2 h at room temperature again. Finally the product was collected, washed and dried as sample Fe. The obtained luminescent magnetic nanocomposite materials were labeled as sample Fe–Ru–Si. For comparison purposes, samples Fe–Si and Si–Ru were also prepared by the same method but samples Ru and Fe were not added to the solution, respectively.

2.2. Measurements

The x-ray diffraction (XRD) patterns were obtained on a Rigaku D/Max-Ra x-ray diffractometer using a Cu target radiation source ($\lambda = 1.5418$ Å). The energy-dispersive x-ray analysis (EDAX) and field-emission scanning electron microscopy (FE-SEM) images were measured on a Hitachi S-4800 microscope. The transmission electron microscopy (TEM) images and the selected-area election diffraction (SAED) pattern were obtained with a JEM-2010 transmission election microscope made by the Japanese company JEOL. The fluorescence image of sample Fe–Ru–Si was recorded by a Nikon TE2000-U fluorescence microscope upon green light excitation. The IR absorption spectra were measured in the range 400–4000 cm^{-1} using a FT-IR spectrophotometer (model Bruker Vertex 70 FT-IR) with a resolution of ± 4 cm^{-1} using the KBr pellet technique. The powder samples were dispersed in absolute ethanol by ultrasonics to form a uniform suspension for the measurements of the UV–vis absorption spectra, which were performed on an UV-3101PC UV–vis–NIR scanning spectrophotometer (Shimadzu) at room temperature. Magnetic characteristics were studied using a vibrating sample magnetometer (VSM) (Lake Shore) at room temperature. The photoluminescent emission spectra were recorded at room temperature with a Hitachi F-4500 spectrophotometer equipped with a continuous 150 W Xe-arc lamp. Thermogravimetric analysis (TGA) was performed up to 600 °C at a heating rate of 10 °C min^{-1} in a flowing nitrogen atmosphere on a Perkin-Elmer-TGA 7 analyzer. In the measurements of temperature dependence of fluorescence, the samples were placed into a liquid nitrogen cycling system (pellet). A continuous 325 nm light from a He–Cd laser was used as the excitation source. The fluorescence was measured by a UV-Lab Raman Infinity (Jobin Yvon) with a resolution of 2 cm^{-1}. In the fluorescence dynamics measurements, a 355 nm light generated from the Nd^{3+}:YAG laser combined with a fourth-harmonic generator was used as the pump, with a repetition frequency of 10 Hz and pulse duration of 10 ns. A two-channel Tektronix TDS-3052 oscilloscope was used to record the fluorescence decay curves. The oxygen-sensing properties of the obtained samples were discussed on the basis of the photoluminescence intensity quenching instead of the excited-state lifetime because it is hard to obtain the precise excited-stated lifetime values under quenched conditions. The oxygen-sensing properties based on luminescence intensity quenching of sample Fe–Ru–Si were characterized using the same Hitachi F-4500 fluorescence spectrophotometer. For measurement of the Stern–Volmer plot, oxygen and nitrogen were mixed at different concentrations via gas flow controllers and passed directly to the sealed gas chamber. We typically allowed 1 min between changes in the N_2/O_2 concentration to ensure that a new equilibrium point had been established. The time-scanning curves were obtained using the same method.

3. Results and discussion

3.1. XRD patterns

Figure 2 shows the XRD patterns of samples Fe and Fe–Si–Ru. Their diffraction peaks corresponded to the rhombohedral structure of Fe_2O_3, but the (018) peak did not appear in the XRD pattern of sample Fe–Si–Ru. Sample Fe–Si–Ru was coated with a SiO_2 shell which may shield diffraction of Fe_2O_3 to a certain extent, and so the intensity of the (018) diffraction peak was too weak to be measured.

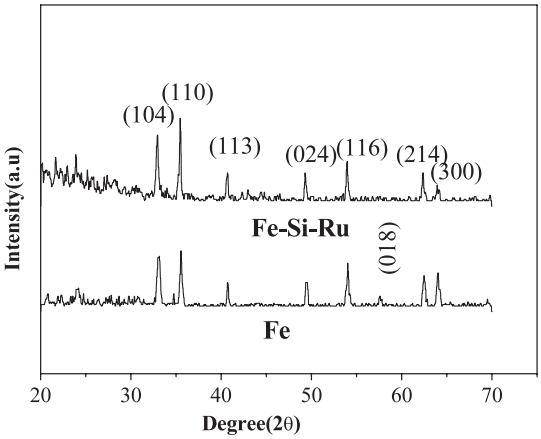

Figure 2. XRD patterns of samples Fe and Fe–Si–Ru.

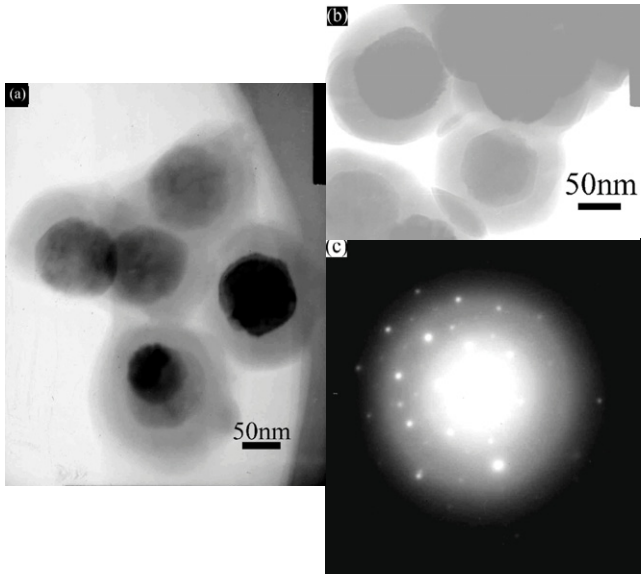

Figure 3. (a), (b) TEM images and (c) SAED pattern of sample Fe–Si–Ru.

3.2. Structure and morphology

The obtained Fe_2O_3 nanoparticles with a mean diameter of ∼115 nm are uniform and monodisperse, making possible the next coating procedure (figure S1, available at stacks.iop.org/Nano/19/495709). The TEM images of sample Fe–Si–Ru are shown in figures 3(a) and (b). No pure SiO_2 particles were found, indicating that Fe_2O_3 nanoparticles were successfully coated with a SiO_2 shell with a thickness of ∼30 nm which can be altered by changing the TEOS concentration. The electron diffraction of sample Fe–Si–Ru (figure 3(c)) shows mixed patterns of polycrystalline Fe_2O_3 and amorphous SiO_2 [32]. The fluorescence image of sample Fe–Si–Ru shows bright red emission of Ru(II) complex arising from the MLCT excited state, proving that the Ru(II) complex was doped into SiO_2 shell (figure S2, available at stacks.iop.org/Nano/19/495709). The EDAX pattern of sample Fe–Si–Ru (figure S3, available at stacks.iop.org/Nano/19/495709) included the peaks of Ru, N, C, Si, further confirming that the Ru complex was doped into SiO_2 and SiO_2 successfully coated bare Fe_2O_3 nanoparticles.

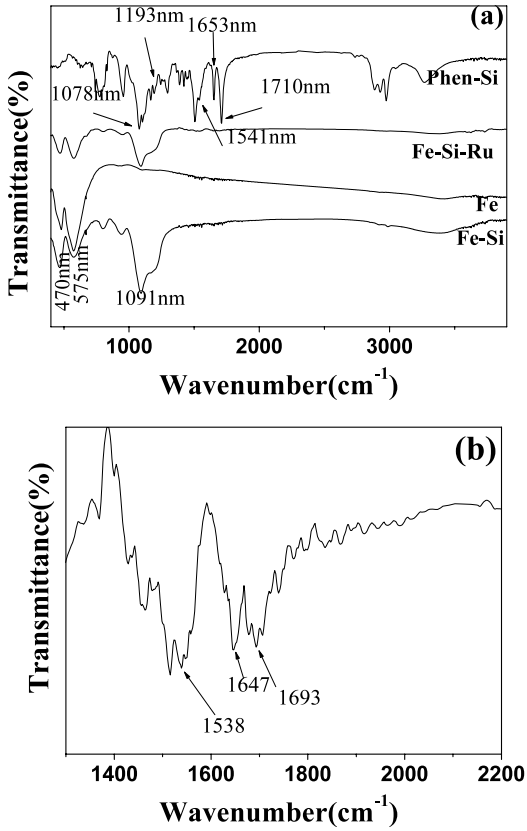

Figure 4. (a) FT-IR spectra of Phen–Si, samples Fe, Fe–Si–Ru and Fe–Si. (b) Amplified FT-IR spectrum of sample Fe–Si–Ru.

3.3. FT-IR spectra

The presence of Ru(II) complexes covalently bonded onto the SiO_2 shell was characterized by IR spectroscopy (figure 4). In the IR spectrum of Phen–Si, the peaks located at 1653 and 1541 cm^{-1} correspond to the –CONH– group. The peaks at 470 and 570 cm^{-1} are characteristic of the Fe–O vibrations for samples Fe, Fe–Si–Ru and Fe–Si [33]. The absorption peak at 1091 cm^{-1} (ν_{as}, Si–O–Si) in samples Fe–Si–Ru and Fe–Si substantiates the formation of a SiO_2 framework [34, 35]. The IR spectrum of sample Fe–Si–Ru was magnified from 1300 to 2200 cm^{-1} (figure 3(b)). The appearance of the peaks located at 1538, 1647 (the vibrations of –CONH–) and 1693 cm^{-1} (the vibration of –C=O–) in sample Fe–Si–Ru is sufficient to prove that the Ru complex was successfully covalently bonded onto SiO_2 networks. In addition, the peaks at 1538, 1647 and 1693 cm^{-1} in sample Fe–Si–Ru showed obvious red-shifts compared to 1541, 1653 and 1710 cm^{-1} for free Phen–Si. The complexation between $Ru(Phen)_2Cl_2$ and the Phen–Si ligand leads to a decrease in their vibration frequencies, which is responsible for the red-shift of the spectra.

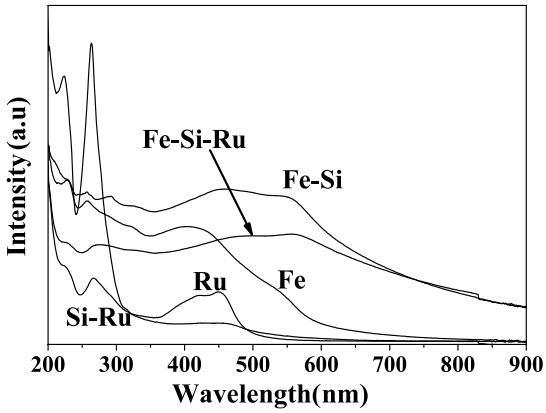

Figure 5. UV–vis absorption spectra of samples Ru, Fe, Fe–Si and Fe–Si–Ru.

3.4. UV–vis absorption spectra

Figure 5 shows the UV–vis absorption spectra of various samples dispersed in ethanol. It can be seen that the pure Ru(II) complex shows two absorption bands centered at 263 and 434 nm. The band at higher energy can be attributed to the ligand centered ($\pi \rightarrow \pi^*$) transition of Phen and the low energy absorption band is assigned to the singlet MLCT ($t_{2g}(Ru) \rightarrow \pi^*(L)$ transition [36]. These two absorption bands were also found in the absorption spectra of samples Si–Ru and Fe–Si–Ru. Sample Fe–Si–Ru contains only a minor amount of Ru and the absorption of Fe_2O_3 is also in this range. For sample Fe–Si–Ru, the absorption band in the range of 355–520 nm is tentatively attributed to an admixture of Ru MLCT transition and Fe_2O_3 absorption.

3.5. Magnetic properties

The magnetic properties of samples Fe and Fe–Si–Ru were studied with fields of up to 3000 G at room temperature (figure 6). Field-dependent magnetization plots illustrated that samples Fe and Fe–Si–Ru are both hysteretic. The magnetic hysteresis loop is large, depicting the strong magnetic response to a varying magnetic field. The coercivities of samples Fe and Fe–Si–Ru were 154 and 130 G, respectively. The decrease in coercivity in sample Fe–Si–Ru can be attributed to the changes in the surface of Fe_2O_3 caused by SiO_2 [37]. The remnant magnetization (M_r) to saturation magnetization (M_s) ratios of samples Fe and Fe–Si–Ru were 0.258 and 0.346, respectively.

3.6. Photoluminescence

The photoluminescent emission spectra of samples Fe–Si–Ru, Fe–Si, Si–Ru in the solid states and Ru in water are shown in figure 7. The broad emission band centered at 590 nm for sample Ru can be attributed to the transition from the triplet MLCT excited state (^{3}MLCT) to the ground state [38]. The emission maximums in samples Fe–Si–Ru and Si–Ru were also almost at this position. No emission at 590 nm was observed from sample Fe–Si and the suspension after sample Fe–Si–Ru has been removed by centrifugation, indicating that all the Ru(II) complex was successfully doped

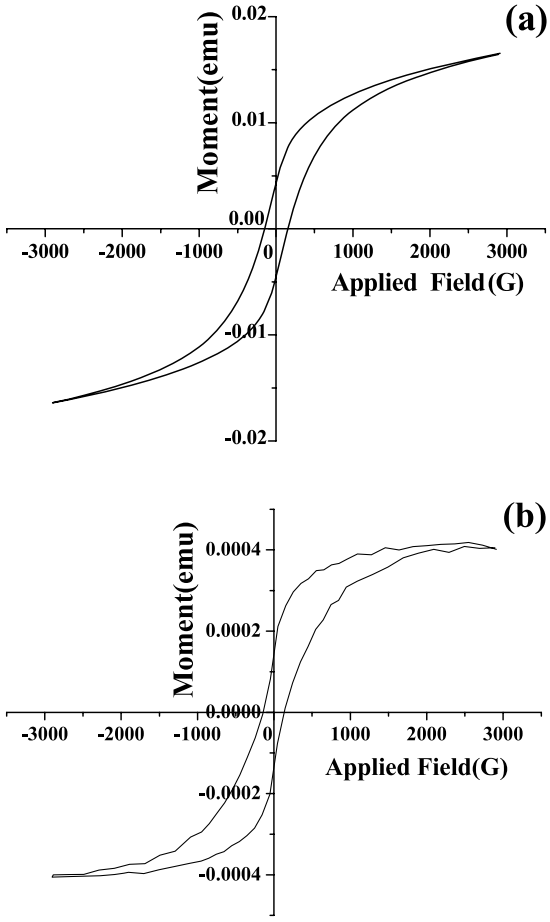

Figure 6. Field-dependent magnetization hysteresis loops of (a) sample Fe and (b) sample Fe–Si–Ru.

into the SiO_2 shell. The thermodynamic stabilities of photoluminescence were also studied in samples Si–Ru and Fe–Si–Ru (see figure S4 in supporting information, available st stacks.iop.org/Nano/19/495709). The results demonstrate that the thermodynamic stability of photoluminescence was improved in the magnetic–photoluminescent–oxygen-sensing nanocomposites than that in the silica gels. The TGA curves of samples Ru and Fe–Si–Ru (not given here) show that both began to decompose at ∼300 °C, indicating that the thermal stability of the Ru incorporated in Fe–Si–Ru was retained.

3.7. Fluorescence lifetime

The fluorescence decay curves of samples Fe–Si–Ru and Si–Ru in solid states and Ru in ethanol were measured at room temperature in the ambient atmosphere. The fluorescence decay curve in sample Ru could be fitted to a single-exponential decay curve expressed by

$$I(t) = \alpha \exp(-t/\tau) \tag{1}$$

where $I(t)$ is the fluorescence intensity at time t, τ the decay time and α the pre-exponential factor. However, the fluorescence decay data in samples Fe–Si–Ru and Si–Ru could be fitted very well to biexponential decay curves expressed by

$$I(t) = a_1 \exp(-t/\tau_1) + a_2 \exp(-t/\tau_2) \tag{2}$$

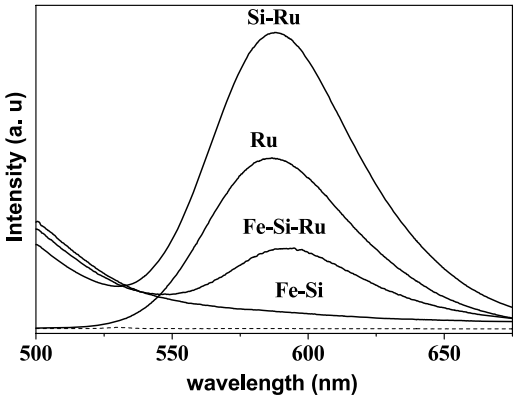

Figure 7. Photoluminescent emission spectra of samples Ru, Fe–Si, Fe–Si–Ru and the suspension after sample Fe–Si–Ru was removed by centrifugation (the dashed line).

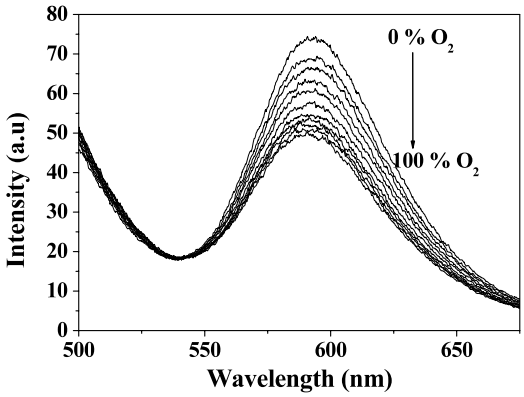

Figure 8. Emission spectra of sample Fe–Si–Ru under different oxygen concentrations.

Table 1. Time-resolved intensity decay constants for various samples.

Sample	a_1	τ_1 (μS)	a_2	τ_2 (μS)	τ (μS)	r^2
Ru	0.472	0.182				0.9988
Fe–Si–Ru	0.286	0.143	0.115	1.024	0.397	0.9985
Si–Ru	0.144	0.251	0.137	1.413	0.593	0.9988

where the subscripts 1 and 2 denote the assigned lifetime components and a_i denotes the pre-exponential factors. The weighted mean lifetime τ_m can be calculated by using the following equation [39]:

$$\langle \tau_m \rangle = \sum_{i=1}^{2} a_i \tau_i \Big/ \sum_{i=1}^{2} a_i. \tag{3}$$

The results of the lifetime measurements are summarized in table 1, showing that the weighted mean lifetimes in samples Fe–Si–Ru and Si–Ru became longer than that in sample Ru dissolved in ethanol. The lifetime can be written as

$$\tau = \frac{1}{W_r + W_{nr}} \tag{4}$$

where W_r and W_{nr} are the total radiative transition rate and the nonradiative rate, respectively. When sample Ru was dissolved in ethanol, the high frequency (O–H) modes around 3400 cm^{-1} can take the role of energy acceptors in the nonradiative decay of MLCT excited states [40, 41]. The increase of lifetimes in samples Fe–Si–Ru and Si–Ru can be attributed to the decrease in the υ(O–H) modes, which decreases the nonradiative rate. The weight per cent of Fe_2O_3 in sample Fe–Si–Ru is 53.85%, and the magnetic Fe_2O_3 as a luminescent killer increases the nonradiative relaxation rate, resulting in a shorter weighted mean lifetime than that in sample Si–Ru.

3.8. Oxygen-sensing properties

The photoluminescence of most Ru(II) complexes could be quenched effectively by molecular oxygen. The room temperature emission spectra under different concentrations of oxygen for sample Fe–Si–Ru are presented in figure 8. The position and shape of MLCT emission from the Ru(II) complex was constant in sample Fe–Si–Ru under different oxygen concentrations. However, the relative luminescent intensity decreased with increasing oxygen concentration, which means than the luminescence intensity of the magnetic–photoluminescent–oxygen-sensing nanocomposites was sensitive to oxygen concentration. Optical sensors based on the luminescence quenching intensity or lifetime of a fluorophore can be examined by Stern–Volmer analysis [42]. In homogeneous media with a single-exponential decay, the intensity form of the Stern–Volmer equation with dynamic quenching is as follows:

$$I_0/I = 1 + K_{SV}[O_2] \tag{5}$$

where I is the fluorescence intensity of the luminophore, the subscript 0 denotes the absence of oxygen, K_{SV} is the Stern–Volmer constant and $[O_2]$ is the oxygen concentration. A plot of I_0/I versus oxygen concentration should give a straight-line relationship with a slope K_{SV}, and an intercept of 1 on the y-axis. However, it is more frequent that the distribution of luminescent species in the solid matrix is heterogeneous on a microscopic scale. In this case, the linear Stern–Volmer quenching curves in equation (5) should be recast as follows:

$$\frac{I_0}{I} = \frac{1}{\frac{f_{01}}{1+K_{SV1}pO_2} + \frac{f_{02}}{1+K_{SV2}pO_2}} \tag{6}$$

where f_{0i} values are the fraction of each of the two sites contributing to the unquenched intensity and K_{SVi} values are the associated Stern–Volmer quenching constants for the two sites. Equation (6) is the familiar Demas 'two-site' model that has proved to have an excellent ability to describe the nonlinear Stern–Volmer quenching curves. Figure 9(a) presents the intensity-based Stern–Volmer plots for sample Fe–Si–Ru. The intensity-based Stern–Volmer oxygen-quenching fitting parameters are also tabulated in table 2. As shown in figure 9(a), sample Fe–Si–Ru shows good linearity. A linear Stern–Volmer plot is very important for an oxygen sensor because it is easy to calibrate and does not require a multipoint calibration strategy when used for practical applications. Figure 9(b) shows the typical dynamic response of sample Fe–Si–Ru upon repeated exposure to nitrogen/oxygen cycles in the

Table 2. Intensity-based Stern–Volmer oxygen-quenching fitting parameters for sample Fe–Si–Ru.

	Stern–Volmer model[a]		Demas two-site model[b]			
Sample	K_{SV} ($O_2\%^{-1}$)	r^2	K_{SV1} ($O\%^{-1}$)	K_{SV2} ($O_2\%^{-1}$)	f_{01}	r^2
Si–Ru	0.0273	0.9931	0.0342	0.000 18	0.9341	0.9988

[a] Terms are from equation (5).
[b] Terms are from equation (6): $f_{01} + f_{02} = 1$.

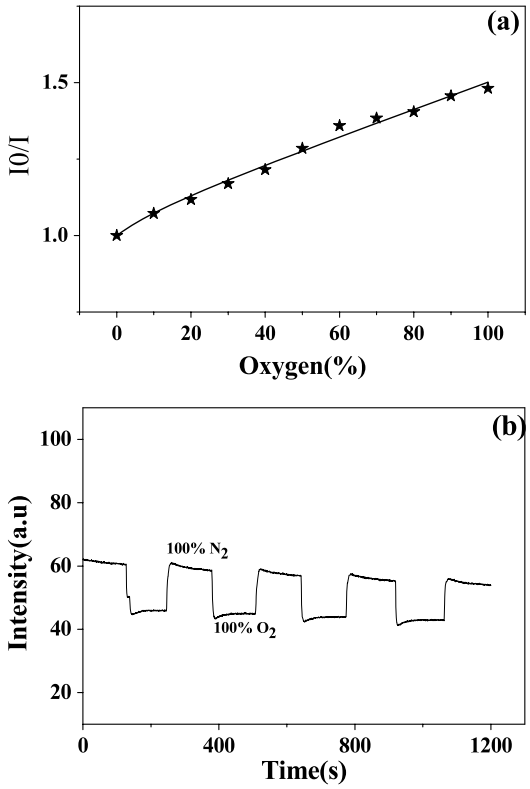

Figure 9. (a) Typical fluorescence intensity-based Stern–Volmer plots for sample Fe–Si–Ru; the solid lines represent the best fit using the Demas two-sites model (equation (6)). (b) Relative luminescence intensity of sample Fe–Si–Ru as a function of time subjected to an atmosphere which was varied periodically between pure N_2 and pure O_2, respectively.

gas phase. The emission intensity transformed quickly when the samples were exposed to different gas phases. However, the luminescence intensity shows a small photobleaching effect under light irradiation, which influenced the stability of the sensor response.

4. Conclusions

In summary, magnetic nanoparticles coated with silica containing a covalently linked ruthenium(II) complex were prepared using a simple solution based method. The nanocomposite materials demonstrated a large magnetic hysteresis loop depicting the strong magnetic response to a varying magnetic field, emitted bright red light and its photoluminescence intensity was sensitive to oxygen concentration. They exhibited better thermal stability of photoluminescent emission compared with the Ru(II) complex in silica gels. A combination of magnetic, photoluminescent and oxygen-sensing properties make them promising candidates for biological applications, such as cell separation, biomarkers and determination of oxygen concentration in biological bodies.

Acknowledgments

The authors gratefully thank the financial supports of One Hundred Talents Project from Chinese Academy of Sciences, the National Natural Science Foundations of China (grant no. 50872130) and Young Teachers of Northeast Normal University (grant no. 20070307).

References

[1] Qian H S, Li Z Q and Zhang Y 2008 *Nanotechnology* **19** 255601
[2] Dong A G, Wang Y J, Tang Y, Ren N, Zhang Y H and Gao Z 2002 *Chem. Mater.* **14** 3217
[3] Xu C J, Xie J, Ho D, Wang C, Kohler N, Walsh E G, Morgan J R, Chin Y E and Sun S H 2008 *Angew. Chem. Int. Edn* **47** 173
[4] López B J, Boissière C, Chanéac C, Grosso D, Vasseur S, Miraux S, Duguet E and Sanchez C 2007 *J. Mater. Chem.* **17** 1563
[5] McBain S C, Yiu H H P, Haj A E and Dobson J 2007 *J. Mater. Chem.* **17** 2561
[6] Hu S H, Liu T Y, Huang H Y, Liu D M and Chen S Y 2008 *Langmuir* **24** 239
[7] Lubbe A S, Bergemann C and Riess H 1996 *Cancer Res.* **56** 4686
[8] Dyal A, Loos K, Noto M, Chang S W, Spagnoli C, Shafi K V P M, Ulman A, Cowman M and Gross R A 2003 *J. Am. Chem. Soc.* **125** 1684
[9] Huang S H, Liao M H and Chen D H 2003 *Biotechnol. Prog.* **19** 1095
[10] Cheng F Y, Su C H, Yang Y S, Yeh C S, Tsai C Y, Wu C L, Wu M T and Shieh D B 2005 *Biomaterials* **26** 729
[11] Tada D B, Vono L L R, Duarte E L, Itri R, Kiyohara P K, Baptista M S and Rossi L M 2007 *Langmuir* **23** 8194
[12] Barbe C, Bartlett J, Kong L, Finnie K, Lin H Q, Larkin M, Calleja S, Bush A and Calleja G 2004 *Adv. Mater.* **16** 1959
[13] Yi D K, Lee S S, Papaefthymiou G C and Ying J Y 2006 *Chem. Mater.* **18** 614
[14] Xu H, Cui L L, Tong N H and Gu H C 2006 *J. Am. Chem. Soc.* **128** 15582
[15] Zheng T H, Pang J B, Tan G, He J B, Mcpherson G L, Lu Y F, John V T and Zhan J J 2007 *Langmuir* **23** 5143
[16] Sivakumar S, Diamente P R and Van Veggel F C J M 2006 *Chem. Eur. J.* **12** 5878
[17] Wang L Y and Li Y D 2006 *Chem. Commun.* **24** 2557
[18] Medintz I L, Uyeda H T, Goldman E R and Mattoussi H 2005 *Nat. Mater.* **4** 435

[19] Lu Y, Yin Y D, Mayers B T and Xia Y N 2002 *Nano Lett.* **2** 183
[20] Yi D K, Selvan T, Lee S S, Papaefthymiou G C, Kundaliya D and Ying J Y 2005 *J. Am. Chem. Soc.* **127** 4990
[21] Santra S S, Zhang P, Wang K, Tapec R and Tan W H 2001 *Anal. Chem.* **73** 4988
[22] Selvan S T, Tan T T and Ying J Y 2005 *Adv. Mater.* **17** 1620
[23] Yu S Y, Zhang H J, Yu J B, Wang C, Sun L N and Shi W D 2007 *Langmuir* **23** 7836
[24] Lu H C, Yi G S, Zhao S Y, Chen D P, Guo L H and Cheng J 2004 *J. Mater. Chem.* **14** 1336
[25] Rossi L M, Shi L F, Quina F H and Rosenzweig Z 2005 *Langmuir* **21** 4277
[26] Lei B F, Li B, Zhang H R, Lu S Z, Zheng Z H, Li W L and Wang Y 2006 *Adv. Funct. Mater.* **16** 1883
[27] Lei B F, Li B, Zhang H R, Zhang L M and Li W L 2007 *J. Phys. Chem.* C **111** 11291
[28] Sullivan B P, Salmon D J and Meyer T J 1978 *Inorg. Chem.* **17** 3334
[29] Kloster G M and Watton S P 2000 *Inorg. Chim. Acta* **297** 156
[30] Seddon K R and Yousif Y Z 1986 *Trans. Met. Chem.* **11** 443
[31] Zhao W R, Gu J L, Zhang L X, Chen H R and Shi J L 2005 *J. Am. Chem. Soc.* **127** 8916
[32] Levy L, Sahoo Y, Kim K S, Bergey E J and Prasad P N 2002 *Chem. Mater.* **14** 3715
[33] Zhang J L, Srivastava R S and Misra R D K 2007 *Langmuir* **23** 6342
[34] Li Y, Yan B and Yang H 2008 *J. Phys. Chem.* C **112** 3959
[35] Yan B and Qiao X F 2007 *J. Phys. Chem.* B **111** 12362
[36] Xia H, Zhu Y Y, Lu D, Li M, Zhang C B, Yang B and Ma Y G 2006 *J. Phys. Chem.* B **110** 18718
[37] Liu K W, Shen D Z, Zhang J Y, Wu X J, Li B H, Li B S, Lu Y M and Fan X W 2006 *J. Cryst. Growth* **297** 390
[38] Innocenzi P, Kozuka H and Yoko T 1997 *J. Phys. Chem.* B **101** 2285
[39] Murtagh M T, Shahriari M R and Krihak M 1998 *Chem. Mater.* **10** 3862
[40] Meyer T J 1986 *Pure. Appl. Chem.* **58** 1193
[41] Caspar J V, Sullivan B P, Kober E M and Meyer T J 1982 *Chem. Phys. Lett.* **91** 91
[42] Zhang H R, Li B, Lei B F, Li W L and Lu S Z 2007 *Sensors Actuators* B **123** 508